Supporting Information

Self-assembly of cobalt(II) and zinc(II) tetranitro octaethylporphyrin *via* bidentate axial ligands: synthesis, structure, surface morphology and effect of axial coordination

Soumyajit Dey, Sk Asif Ikbal and Sankar Prasad Rath*

Department of Chemistry, Indian Institute of Technology Kanpur, Kanpur-208016, INDIA. Email: sprath@iitk.ac.in

Table S1. Crystal Data and Data Collection Parameters

	[**1**]•L^1	[**1**]•L^2	[**2**]$_2$•L^1	[**2**]$_2$•L^2	[**2**]$_2$•L^3
T, K	100(2)	100(2)	100(2)	100(2)	100(2)
Formula	$C_{47.50}$ $H_{49.50}$ $C_{l4.50}$ Co N_{12} O_8	C_{48} H_{48} Co N_{12} O_8	C_{86} H_{92} Cl_{12} N_{20} O_{16} Zn_2	$C_{99.60}$ $H_{121.20}$ N_{20} O_{16} Zn_2	C_{84} H_{90} N_{20} O_{16} Zn_2
Formula weight	1134.95	979.91	2217.94	1985.31	1766.50
Crystal system	Triclinic	Tetragonal	Monoclinic	Monoclinic	Triclinic
Space group	P-1	I 41/a	P21/c	P21/c	P-1
a, Å	12.274(5)	17.158(3)	11.3631(11)	13.9272(19)	12.924(3)
b, Å	13.707(5)	17.158(3)	33.868(3)	37.718(5)	13.663(3)
c, Å	18.913(5)	15.910(5)	26.769(3)	11.3170(15)	13.678(3)
α, deg	107.964(5)°	90	90	90	69.774(4)
β, deg	104.161(5)°	90	101.816(2)	110.296(2)	66.261(4)
γ, deg	98.063(5)°	90	90	90	85.852(4)
V, $Å^3$	2853.4(17)	4683.6(19)	10083.6(17)	5575.8(13)	2068.3(8)
Radiation (λ, Å)	Mo Kα (0.71073)	Mo Kα (0.71073)	Mo Kα (0.71073)	Mo Kα (0.71073)	Mo Kα (0.71073)
Z	2	4	4	2	1
d_{calcd}, g•cm^{-3}	1.321	1.390	1.461	1.182	1.418
μ, mm^{-1}	0.570	0.434	0.865	0.497	0.660
F(000)	1172	2044	4560	2094	922
No. of unique data	10363	2174	17739	9804	7237
No. of params. Refined	612	164	1113	559	558
GOF on F^2	0. 939	1.047	0.969	0.916	1.065
*R*1[a] $[I > 2\sigma(I)]$	0.0815	0.0577	0.0730	0.0524	0.0676
*R*1[a] (all data)	0.1188	0.0771	0.1004	0.0794	0.0799
wR2[b] (all data)	0.2400	0.1615	0.2020	0.1335	0.1974

$$a\ R1 = \frac{\sum ||Fo| - |Fc||}{\sum |Fo|}; \quad b\ wR2 = \sqrt{\frac{\sum \left[w\left(Fo^2 - Fc^2\right)^2\right]}{\sum \left[w\left(Fo^2\right)^2\right]}}$$

Table S2. Selected Bond Distances (Å) and Angles (º)

Bond length, (Å)	**[1]**•L^1	**[1]**•L^2	$[\mathbf{2}]_2$•L^1		$[\mathbf{2}]_2$•L^2	$[\mathbf{2}]_2$•$\mathbf{L}^3$
			core I	core II		
M(1)-N(1)	1.984(4)	1.975(2)	2.059(3)	2.075(3)	2.055(2)	2.076(4)
M(1)-N(2)	1.975(4)		2.079(3)	2.086(3)	2.068(3)	2.083(4)
M(1)-N(3)	1.976(4)		2.092(3)	2.086(3)	2.075(2)	2.079(4)
M(1)-N(4)	1.996(4)		2.073(3)	2.068(3)	2.083(3)	2.077(4)
M(1)-N(5)	2.260(4)	2.291(3)	2.182(3)	2.180(3)	2.182(2)	2.114(4)
M(1)-N(6)	2.277(4)					
Bond angles,(deg)						
N(1)-M(1)-N(2)	89.78(16)		89.70(12)	88.66(12)	89.07(11)	89.13(15)
N(1)-M(1)-N(3)	174.10(14)		168.39(12)	161.64(12)	167.98(9)	155.71(16)
N(1)-M(1)-N(4)	90.82(15)		89.01(13)	89.48(12)	89.82(10)	87.45(15)
N(2)-M(1)-N(3)	90.66(15)		88.79(12)	88.71(12)	88.72(10)	87.70(15)
N(2)-M(1)-N(4)	173.88(14)		161.24(12)	168.55(12)	161.47(9)	162.72(16)
N(3)-M(1)-N(4)	89.36(15)		88.72(12)	89.51(12)	88.53(9)	88.48(15)
N(1)-M(1)-N(5)	85.83(14)	86.80(7)	95.53(12)	99.14(11)	95.20(9)	100.34(15)
N(2)-M(1)-N(5)	93.81(15)		98.97(12)	96.06(12)	99.84(10)	95.67(15)
N(3)-M(1)-N(5)	88.27(14)		96.08(12)	99.21(11)	96.82(9)	103.94(15)
N(4)-M(1)-N(5)	92.30(14)		99.78(12)	95.39(12)	98.68(9)	101.61(16)
N(1)-M(1)-N(6)	92.64(14)					
N(2)-M(1)-N(6)	85.82 (14)					
N(3)-M(1)-N(6)	93.26(14)					
N(4)-M(1)-N(6)	88.08(14)					
N(5)-M(1)-N(6)	178.43(14)					

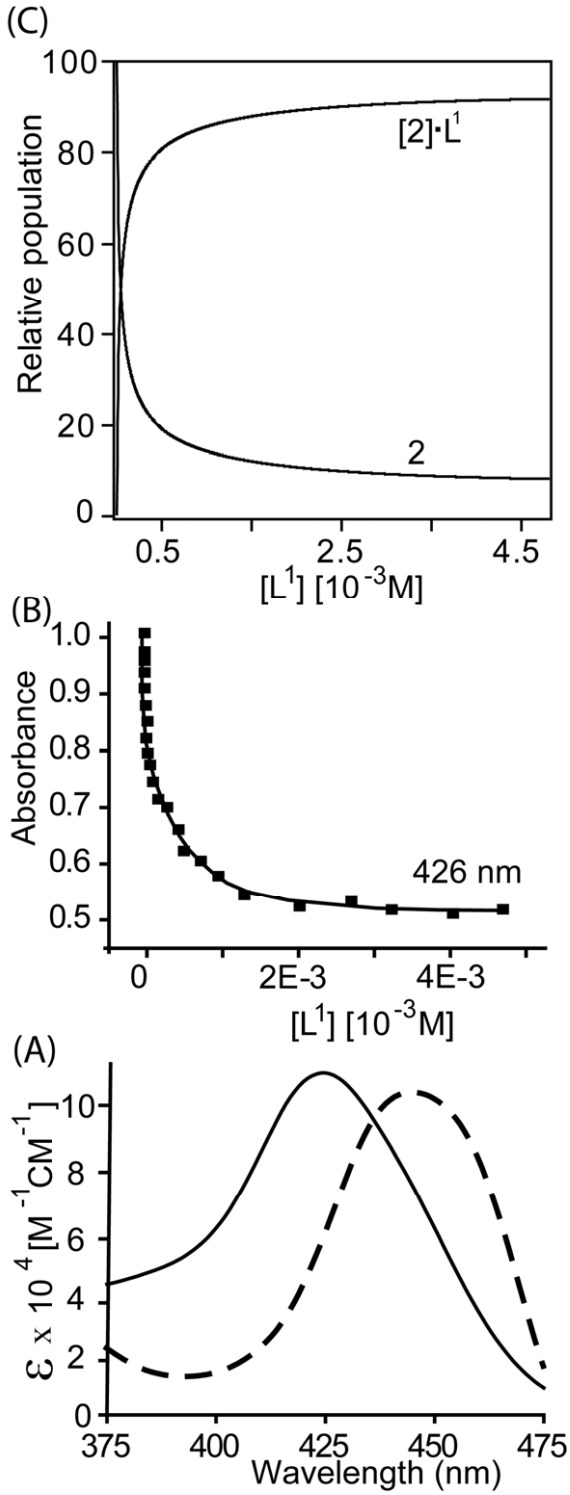

Figure S1. (A) Calculated UV-visible spectra of **2** (solid line) and $[\mathbf{2}]_1 \bullet L^1$ (dashed line) complexes formed between **2** and L^1. (B) Fits of the absorbance data at selected wavelength 426 nm. (C) Species distribution plot of the **2** and $[\mathbf{2}]_1 \bullet L^1$ complexes.

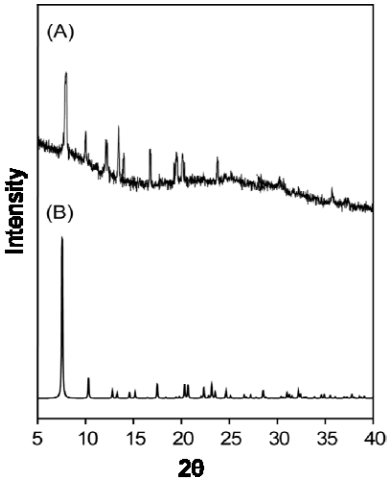

Figure S2. PXRD profiles of [**1**]•L^2: (A) bulk powder sample of the complex at 295 K, and (B) simulated pattern obtained from X-ray structure at 100 K.

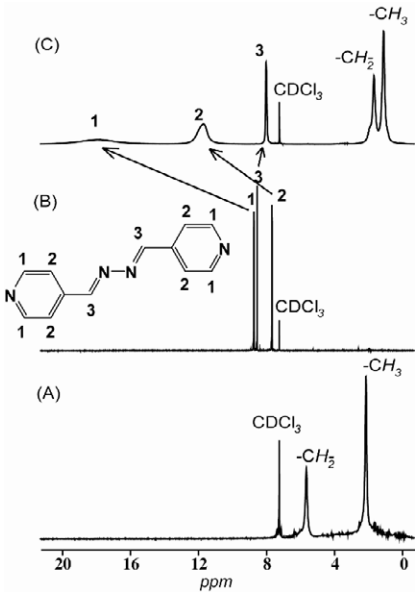

Figure S3. ^{1}H NMR spectra in $CDCl_3$ (at 295 K) of (A) Co^{II}(*tn*-OEP), **1**, (B) L^2, and (C) [**1**]·L^2

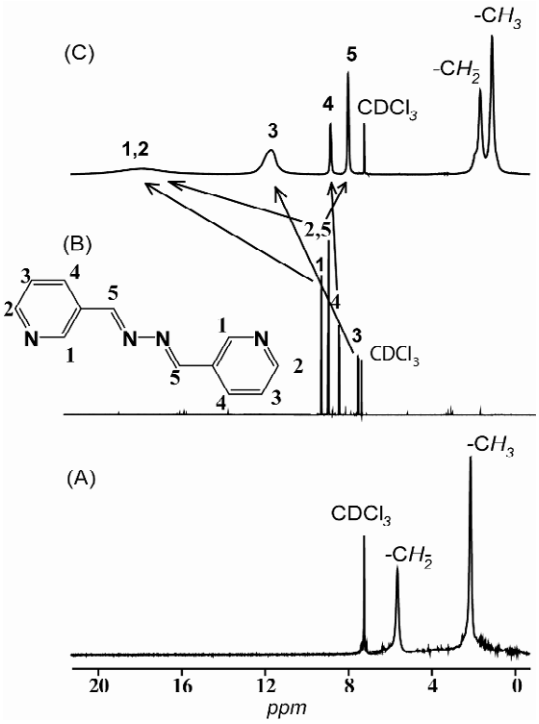

Figure S4. ^{1}H NMR spectra in $CDCl_3$ (at 295 K) of (A) Co(*tn*-OEP), **1**, (B) L^3 and (C) [**1**]·L^3

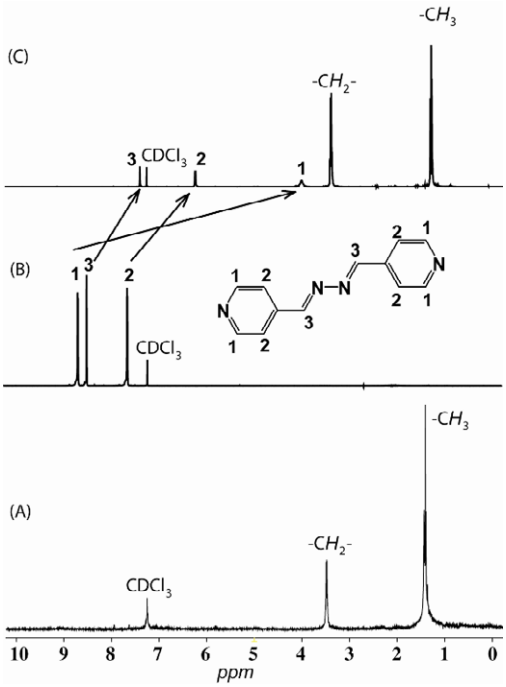

Figure S5. ^{1}H NMR spectra in $CDCl_3$ (at 295 K) of (A) Zn(*tn*-OEP), **2**, (B) L^2, and (C) [**2**]$_2$·L^2

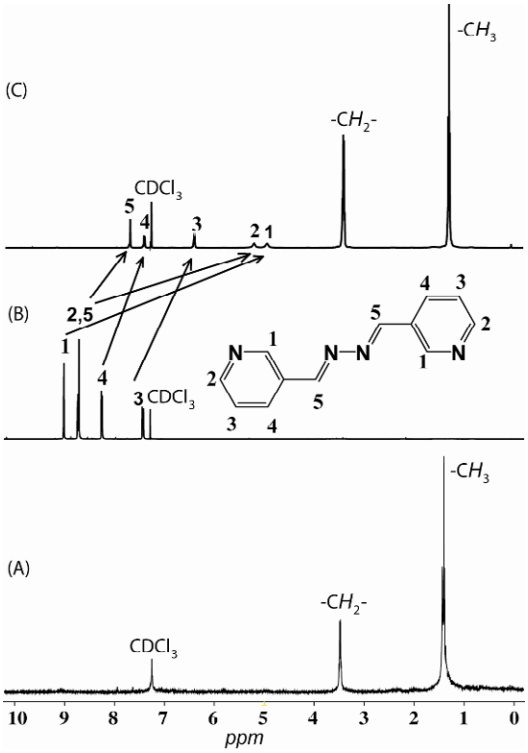

Figure S6. ^{1}H NMR spectra in $CDCl_3$ (at 295 K) of (A) Zn(*tn*-OEP), **2**, (B) L^3 and (C) $[\mathbf{2}]_2 \cdot L^3$.

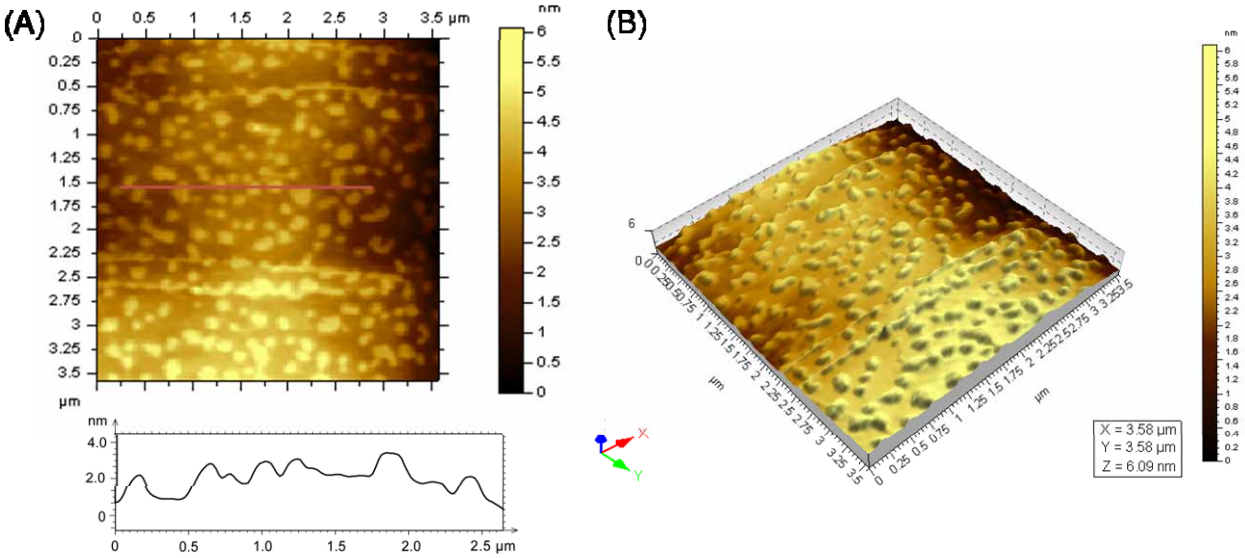

Figure S7. Topographic AFM images and 3D view of $[\mathbf{2}]_2 \bullet L^3$ (A, B) drop cast onto HOPG from $5x10^{-6}$ M solution in tetrahydrofuran. The contours in the frames below the images correspond to the line in the images.

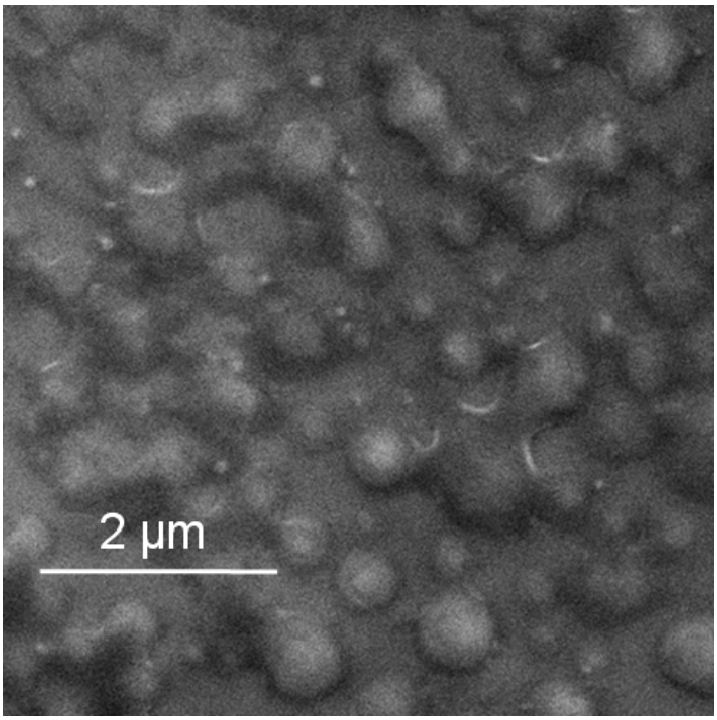

Figure S8. SEM images of $[\mathbf{2}]_2 \bullet L^3$ drop cast onto HOPG from $5x10^{-6}$ M solution in tetrahydrofuran.